Chemical Engineering Journal 156 (2010) 134–140

Contents lists available at ScienceDirect

Chemical Engineering Journal

journal homepage: www.elsevier.com/locate/cej

Adsorption behavior of Li^+ onto nano-lithium ion sieve from hybrid magnesium/lithium manganese oxide

Liyan Tian, Wei Ma*, Mei Han

Department of Chemistry, Dalian University of Technology, Dalian 116023, Liaoning, China

ARTICLE INFO

Article history:
Received 27 June 2009
Received in revised form
28 September 2009
Accepted 2 October 2009

Keywords:
Adsorption
Lithium
Lithium ion sieve
Modeling
Kinetics

ABSTRACT

Magnesium (II) doped spinel lithium manganese oxide (LMS) was synthesized by soft chemical method and nanosized ion sieve manganese oxide (HMS) was prepared by extracting lithium and magnesium from LMS. The characteristics of HMS were studied by X-ray diffraction, scanning electron microscopy, transmission electron microscopy, surface areas and determination of pH at the point of zero charge. Experiments were performed to study the effects of pH, adsorbent dose, contact time and Li^+ concentration. The competitive model was used to describe the competition between Li^+–H^+ and the applicability of different kinetic models was evaluated. The results showed that the pH at the point of zero charge of HMS was about 7.8. The recycle of HMS explained that it could be used as Li^+ adsorbent with topotactical extraction of lithium. Under optimized batch conditions up to 99.2% Li^+ could be recovered from solution within 24 h. The adsorption process followed the pseudo-second-order model and followed an intraparticle diffusion model at the beginning.

1. Introduction

Recently, the demand for lithium has been growing for their promising use in many fields, such as high-performance grease, heat-resistant ceramics, flux for welding, batteries, and pharmaceuticals and so on. Lithium is now recovered from mines and salt lakes, which contain about 17 million tons of lithium in total [1]. Seawater is also considered as a vast source of lithium (about 2.5×10^{11} tonnes), although the concentration of lithium is very low, i.e., 0.17 mg/L [2]. In addition, there is a lot of lithium in waste solution of spent lithium ion batteries which are widely used. In conventional practice, precipitation is the most common technology for lithium recovery. However, it is difficult to apply precipitating method to saline with high Mg/Li, sea and the waste solutions of spent lithium ion batteries with low concentration of lithium, because Li_2CO_3 is insoluble (about 1.3 g/100 mL H_2O) which causes incomplete precipitation [3]. Therefore, the adsorption method has been recognized as the most suitable method for lithium recovery owing to economic and environmental considerations [4].

Spinel-type lithium manganese oxides show excellent selectivity and capacity for the adsorption of Li^+ after topotactic extraction of Li^+ with an acid, such as λ-MnO_2, $MnO_2 \cdot 0.31H_2O$, $MnO_2 \cdot 0.5H_2O$ derived from $LiMn_2O_4$, $Li_{1.33}Mn_{1.67}O_4$, $Li_{1.6}Mn_{1.6}O_4$ respectively [5–10]. The adsorptive properties make the material practicable as a Li^+ adsorbent, a cathode material for lithium batteries and electrode for selective electroinsertion of Li^+ [11]. However, they show significant manganese loss during extraction of lithium by acid [12]. A very effective way for improving the stability is to synthesize manganese-substituted $LiMn_{2-x}M_xO_4$ spinel phase by doping with divalent or trivalent ions (M = Mg, Co, Ni, Fe, Ti, Zn, Cr, etc.) [13–17]. From a practical point of view, HMnO(Mg) has advantages in that one of the raw materials, Mg^{2+}, is non-polluting and can be easily obtained from seawater. Therefore, its cost should be much lower than that of HMnO(Li). Feng et al. [18], Liu et al. [19], Chitrakar et al. [20] and Miyai et al. [21,22] have studied the Li^+ extraction and insertion reactions of $LiM_{0.5}Mn_{1.5}O_4$ (M = Mg, Zn, Al, Sb, etc.), Mg_2MnO_4 and $MgMn_2O_4$. The results implied that their acid treated products had selectivity for Li^+ as doped lithium ion sieves and had potential application for lithium recovery from aqueous phases.

Since the sorption processes often occur in aqueous solutions, it is very important to understand the adsorption behavior of lithium ion sieve. However, recently there have been few systematic studies on the adsorption behavior of Li^+ onto doped lithium ion sieve. Therefore, in this study, Mg^{2+} doped spinel lithium manganese oxide (LMS) and the nanosized ion sieve manganese oxide (HMS) were prepared by soft chemical method based on the preliminary work of our laboratory [23]. The characteristics of HMS were studied by X-ray diffraction (XRD), scanning electron microscopy (SEM), transmission electron microscopy (TEM), surface areas and determination of point of zero charge (PZC). Batch adsorption properties were studied by investigating the effects of different experimental

* Corresponding author. Tel.: +86 411 8470 6303; fax: +86 411 8470 7416.
E-mail address: chmawv@yahoo.com (W. Ma).

1385-8947/$ – see front matter © 2009 Published by Elsevier B.V.
doi:10.1016/j.cej.2009.10.008

parameters including adsorbent dosage, initial pH and adsorption time. The competitive model was applied to describe the competition between Li^+ and H^+. Kinetic measurements were assessed at different Li^+ concentrations and evaluated by the pseudo-second-order model and intraparticle diffusion model.

2. Experimental methods

2.1. Preparation of the material

$MnCl_2{\cdot}4H_2O$ (AR, TianJin Chemicals) and $Mg(NO_3)_2{\cdot}6H_2O$ (AR, TianJin Chemicals) in a Mg:Mn molar ratio of 3:1 were dissolved in proper deionized water, some LiOH (AR, Guangdong Chemicals) solid was dropped into the mixed solution to adjust the pH of mother solution over 11 with 200 rpm magnetic stirring. After about half an hour, H_2O_2 (AR, Shenyang Chemicals) with a mass concentration of 15–20% was added dropwise into the above solution. A black gel was formed after continuously stirred for 2 h. The obtained black gel was dried in an evaporating dish at 80 °C for several hours and then heated at 450 °C for 4 h. The obtained sample was cooled and designated as LMS then stirred in 0.5 mol/L hydrochloric acid for 24 h. The acid-treated material was filtered, washed with deionized water and dried at 80 °C. The Li^+ extraction sample was designated as HMS.

2.2. Analytical methods

The material thus synthesized was characterized by the following methods. Powder X-ray diffraction (XRD) analysis was carried out to identify the phase of the material using a Shimadazu XRD-6000 X-ray diffractometer with Cu Kα radiation (λ = 1.5406 Å) monochromated by graphite at 40 kV and 30 mA, scanning from 5° to 70° at the speed of 0.06° s^{-1}.

The grain morphology and particle size were observed by scanning electron microscopy (SEM, JEOL JSM-5600LV) and transmission electron microscopy (TEM) on a JEOL 2200FS at accelerating voltage of 200 kV and photomicrographs collected using a Hamamatsu CCD digital camera. Surface areas of the materials were measured by the BET method with a NOSA 1001 specific surface analyzer.

The atomic absorption spectrophotometer (Solan 969 USA) was used for determination of initial and final Li^+ concentrations. The wavelength used for the analysis of Li was 670.8 nm.

Batch equilibration technique was applied to determine pH at the point of zero charge (pH_{PZC}) [24]. NaCl was selected as an inert electrolyte and the ionic strength was kept constant in all experiments. Portions of ion sieve powder were introduced into a known volume (50 mL) of 0.1 mol/L and 0.01 mol/L NaCl solution respectively. Initial pH values ($pH_{initial}$) of NaCl solutions were adjusted from about 2 to 12 by addition of 0.1 mol/L HCl or NaOH. Suspensions of the same sorbent to solution ratio (1 g/5 L) were allowed to equilibrate for 24 h in a shaker thermostated at 20 °C. Then the suspensions were filtered through a filter paper and the final pH values (pH_{final}) were measured again. pH_{PZC} of HMS was determined from the plots pH_{final} versus $pH_{initial}$.

2.3. Batch experiments

Adsorption of Li^+ onto HMS was studied in batch system, and the parameters affecting the adsorption process such as adsorbent dose, initial pH, initial Li^+ concentration and contact time were investigated. The Li^+ solution was prepared by dissolving LiCl (AR, TianJin Chemicals) in deionized water. The adsorbent concentration was changed from 0.5 to 3.5 g/L in order to seek the optimum adsorbent dosage for adsorption of Li^+ by HMS. Sorbent–sorbate mixture was then centrifuged at 3500 rpm for 5 min, and the remaining Li^+ concentration in the supernatant was determined. The same procedure stated here was carried out for determination of Li^+ concentrations in solutions for all batch adsorption studies. The effect of initial pH of the Li^+ solution on the adsorption capacity of HMS was investigated in the pH range of 2–12. The pH of the solution was adjusted with diluted hydrochloric acid and sodium hydroxide solutions using a pH meter. Batch studies were carried out by mixing HMS with LiCl solution at different $pH_{initial}$ (2–12) and shaking in a rotary shaker with glass flasks. All of the parameters, adsorbent concentration (1 g/L), temperature (20 °C), initial Li^+ concentration (10–200 mg/L), and contact time (24 h), were kept constant respectively at each pH value. In this procedure, the effect of initial Li^+ concentration was included synchronously. Finally, the adsorption equilibrium time profile (at $pH_{initial}$ 12) was examined in the time range of 1–48 h as a function of Li^+ concentration (10–100 mg/L) in order to understand the adsorption behavior of HMS. The intraparticle diffusion kinetic, pseudo-second-order and pseudo-first-order models were applied to the obtained data.

In this study, all chemicals were analytical reagent grade. Deionized water was used throughout the study. All the experiments were performed in duplicates and the deviation about the mean was less than five percent in all cases.

Adsorption capacity values will be calculated from the change of solution concentration using the following equation:

$$q_e = \frac{(c_0 - c_e) \times V}{w} \quad (1)$$

where q_e is the adsorption amount (mg/g) and c_0 and c_e are the initial and final concentrations (mg/L), respectively. V is the volume of solution (L) and w is the mass of adsorbent used (g).

2.4. Models

2.4.1. Competitive adsorption model

The most common models used for sorption processes are the Langmuir and Freundlich isotherms. The major advantage of these models is their simplicity [25]. However, both models fail to predict the effects of several important factors such as pH. If the model parameters are obtained based on experiments under one set of conditions, the models cannot give accurate predictions for another set of conditions [26]. Some researchers have been developed competitive adsorption isotherms in order to take into account the sorption of H^+ [27], such as Eq. (2).

$$q = \frac{(q_{max}/K_{Li})C_f[Li]}{1 + (1/K_{Li})C_f[Li] + (1/K_H)C_f[H]} \quad (2)$$

where C_f is the equilibrium metal ion concentration (mmol/L), K_H is the equilibrium constant for the binding of proton (mmol/L), K_{Li} is the equilibrium constant for the binding of lithium (mmol/L), q_{max} is the maximum amount of adsorption (mmol/g) and q is the amount of metal bound to the HMS (mmol/g).

2.4.2. Intraparticle diffusion kinetics

In order to investigate the mechanism of the adsorption of Li^+ onto HMS, an intraparticle diffusion based mechanism has been studied. The intra-mass transfer diffusion model proposed by Weber and Morris is used for intraparticle transfer, which is determined by the linear equation [28]:

$$q_t = k_{WM} t^{1/2} + C \quad (3)$$

where q_t (mg/g) is the amount of adsorption at time t (h), C is the intercept (mg/g) and k_{WM} is the intraparticle diffusion rate constant of Weber and Morris (mg/(g $h^{1/2}$)). It can be used to analyze deferent period of adsorption process. k_{WM} and C are obtained from a linear regression analysis.

2.4.3. The pseudo-second-order kinetics

The pseudo-second-order kinetic model is expressed as [29]:

$$\frac{t}{q} = \frac{t}{q_e} + \frac{1}{k_2 q_e^2} \tag{4}$$

where k_2 (g mg^{-1} h^{-1}) is the rate constant of second-order adsorption. The second-order rate constant k_2 and q_e are calculated from the intercept and slope of the plots of t/q versus t.

2.4.4. Non-linear regression analysis

In this study the parameters were evaluated by non-linear regression by Matlab 7.1. The optimization procedure required an error function to be defined in order to evaluate the fit of the equation to the experimental data. Not only the determination coefficient (R^2) but also the residual root mean square error (RMSE) and the sum of the squared errors (SSE) were used to measure the goodness-of-fit. RMSE can be defined as [30]:

$$\text{RMSE} = \sqrt{\frac{1}{m-2}\sum_{i=1}^{m}(Q_i - q_i)^2} \tag{5}$$

where Q_i is the observation from the batch experiment and q_i is the estimate from the isotherm for corresponding Q_i and m is the number of observations in the experimental isotherm. The smaller RMSE value indicates the better curve fitting.

The parameters of the equations were determined by minimizing the distance between the experimental data points and the models predictions. SSE can be presented as:

$$\text{SSE} = \sum_{i=1}^{n}(q_{\text{exp},i} - q_{\text{cal},i})^2 \tag{6}$$

where $q_{\text{exp},i}$ is the equilibrium value obtained from the batch experiment and $q_{\text{cal},i}$ is calculated by models. If data from the model are similar to the experimental data, SSE value will be a small number; if they are different, SSE will be a large number [31].

3. Results and discussion

3.1. Characterization of LMS and HMS

Mg^{2+} doped spinel lithium manganese oxide (LMS, $LiMg_{0.56}Mn_{1.50}O_4$) was synthesized by soft chemical method and the ion sieve manganese oxide (HMS, $H_{1.51}Li_{0.08}Mg_{0.24}Mn_{1.49}O_4$) was prepared by extracting lithium and magnesium from LMS. X-ray diffraction patterns of lithium magnesium manganese oxide and acid-treated sample (HMS) are shown in Fig. 1. They all show

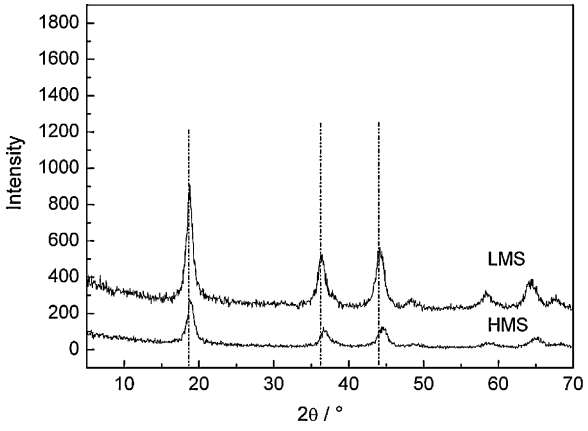

Fig. 1. X-ray diffraction patterns of precursor and acid-treated sample.

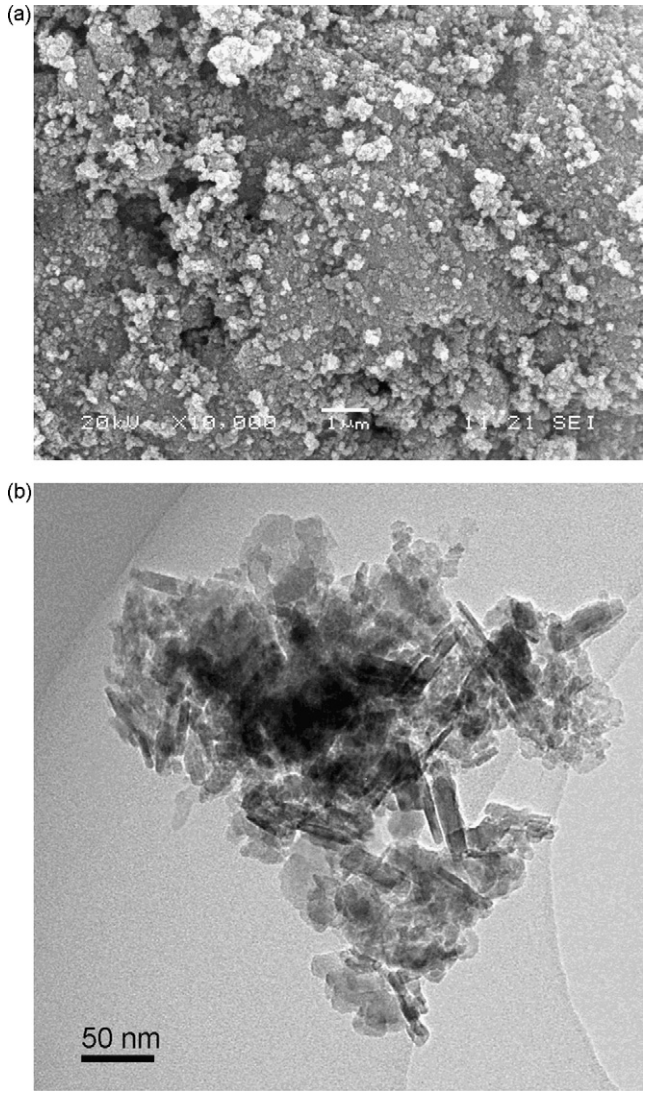

Fig. 2. SEM image (a) and TEM image (b) of HMS.

the pure spinel structure, viz. the diffraction patterns of delithiated material are almost the same as that of the precursor, only with relative intensities slightly weaker and the peaks shifted to slightly higher 2θ values [32]. This indicates that lithium extraction proceeds topotactically, preserving the original spinel structure, while increasing slightly in grain size during the extraction of lithium. The lithium extraction from LMS is similar to that from lithium manganese oxide [6,8].

Fig. 2 shows the SEM and TEM images of HMS. It can be seen from SEM image that the lithium ion sieve is composed of dispersed particles and their aggregates. The HMS grains present as the cluster form of floccules. The TEM image clearly shows that HMS has clubbed structures with about 25 nm × 50 nm and nanosized particles. The BET surface area of HMS is 131.8 m^2/g. Smaller size provides bigger surface area and helps to the adsorption of Li^+.

The pH_{PZC} is defined as the solution pH value for which the free surface charge of the colloidal particles is zero [33]. For oxide colloidal systems, the H^+ and OH^- are considered to be the potential determining ions. Since the charge on HMS surface is a result of the adsorption of H^+ and OH^- ions, as well as of dissolution and hydrolytic reactions occurring at the solid–solution interface [34], the pH_{PZC} is dependent on the solid to solution ratio (surface area). So suspensions of the same solid to solution ratio (1 g/5 L) were

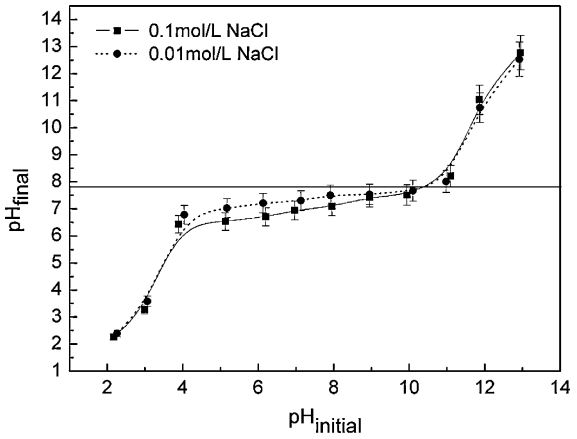

Fig. 3. pH_{final} as a function of $pH_{initial}$ for solid to solution ratio 1 g/5 L (experimental conditions: temperature, T = 20 °C; HMS mass, m = 0.05 g; volume of NaCl, V_{NaCl} = 250 mL).

carried out through all the adsorption experiments. Fig. 3 shows pH_{final} vs $pH_{initial}$ curves at different electrolyte concentrations and the pH_{PZC} of HMS is around 7.8 as revealed by the crossing point of the curves which shows an amphoteric HMS surface. There is a reasonable prediction that positively charged sites with anions adsorbed are predominant when pH is lower than 7.8, while negatively charged sites with cations adsorbed are predominant when pH is higher than 7.8. Therefore, there are electrostatic forces during the sorption of Li^+ onto HMS in addition to the main ion-exchange mechanism.

3.2. The effect of HMS dose on recovery of Li^+

Adsorbent dose seems to have a great influence in adsorption process because the dose of adsorbent added into the solution determines the number of binding sites available for adsorption [35–37]. In addition, it also determines the number of Li^+ insertion sites. The results are shown at Fig. 4. It indicates that the adsorption capacity decreases with the increase of ion sieve dose from 0.05 to 0.35 g. This may be explained by several factors such as unsaturation of adsorption sites and particle interaction. However, it is evident from the figure that the removal increases from 79.1 to 99.2%, which is due to the increase in absorbent surface area of the adsorbent. The further increase of adsorbent dose from 1.0 g/L does not significantly improve adsorption due to establishment of equilibrium between adsorbent and Li^+.

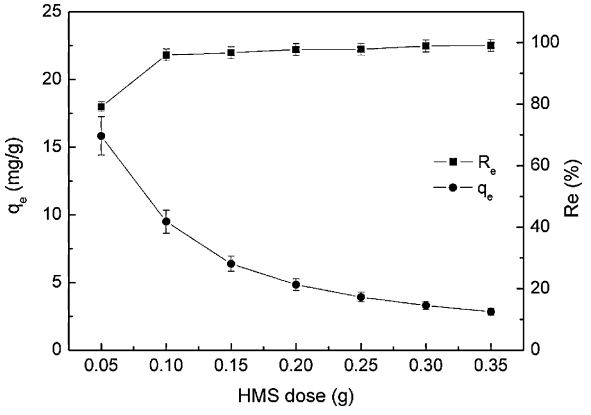

Fig. 4. The effect of ion sieve dose on adsorption of Li^+ (T = 20 °C; m = 0.05–0.35 g; volume of lithium solution, V = 100 mL; initial concentration of lithium, C_0 = 10 mg/L; $pH_{initial}$ = 12).

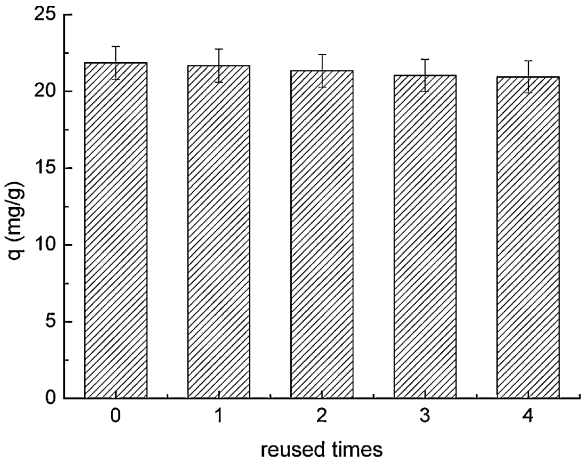

Fig. 5. Relation of reuse times and adsorption capacity (T = 20 °C; V = 250 mL; C_0 = 10 mg/L; $pH_{initial}$ = 12).

3.3. Recycle of the ion sieve

The relation of reused times and adsorption capacity is shown in Fig. 5. The adsorption capacity decreases slightly with the increase of reused times. This attributes to slight damage to the original cubic structure when the extraction of Li^+ and Mg^{2+} from LMS proceeds by means of an acid treatment. While the adsorption capacity stays at 21–22 mg/g with the initial concentration 10 mg/g and after reused for 4 times, it remains above 95% higher than HMnO(Mg) which was reported as 60% [21]. It indicates that HMS is found to have a higher chemical stability and the lithium ion sieve could be recycled in the lithium ion solutions for recovery of lithium. It dues to the substitution of monovalent, divalent, trivalent or pentavalent cations for some portions of the manganese ions in the spinel framework and the doped magnesium ions reduce the dissolution of manganese ions [8]. The Li^+ and Mg^{2+} extraction and the Li^+ insertion reactions mainly proceed by an ion-exchange-type mechanism [18].

3.4. Effect of initial pHs and concentrations

It is known that solution pH and initial concentration can significantly influence the adsorption of metal ions, the same as Li^+ adsorption by ion sieve. Fig. 6 is the curve of Li^+ adsorption in different initial pHs and solution concentrations but at the

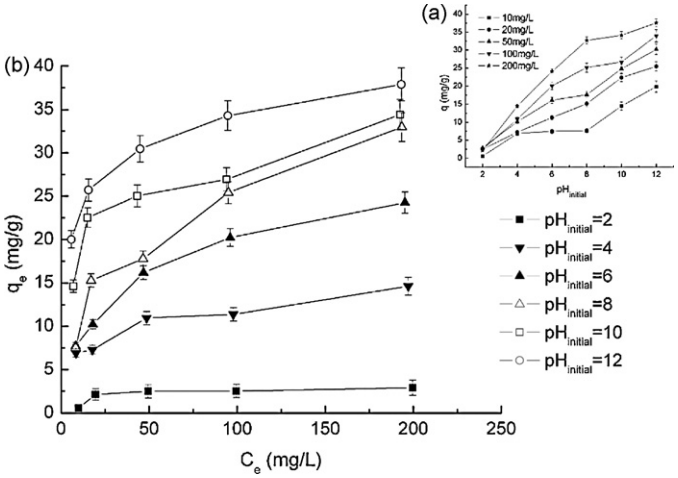

Fig. 6. Variation of Li^+ adsorption in different initial pHs and concentrations (T = 20 °C; m = 0.05 g; V = 250 mL; C_0 = 10–200 mg/L; $pH_{initial}$ = 2–12).

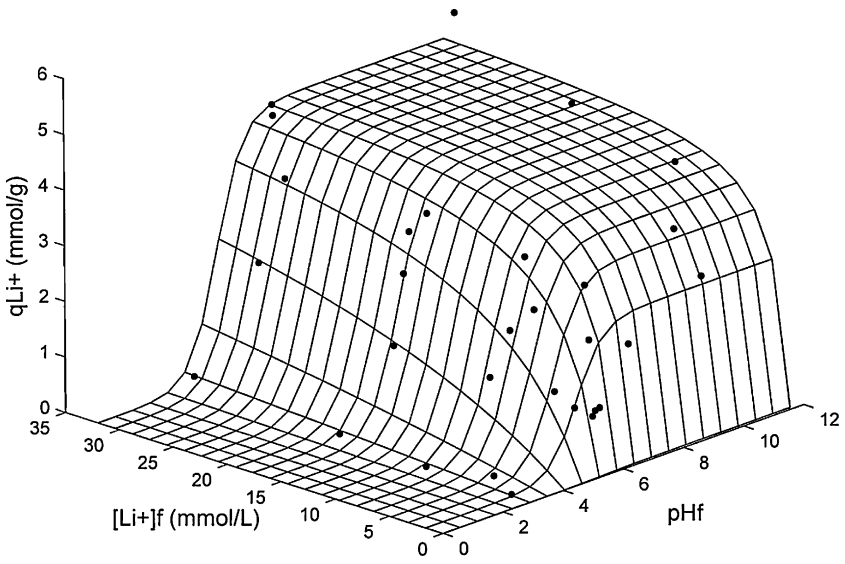

Fig. 7. The competitive model of Li–H binary system (T = 20 °C; m = 0.05 g; V = 250 mL; C_0 = 10–200 mg/L; $pH_{initial}$ = 2–12).

same temperature (20 °C). It shows that adsorption capacity of Li^+ increases both with increasing pH and generally with increasing solution concentration. The shape of the isotherm implies that there is affinity between Li^+ and HMS. From Fig. 6a, it can be seen that the adsorption capacity is thus highly pH-dependent. It reaches up to 37.4 mg/g when the initial concentration is 200 mg/g at pH 12 which is higher than that of Mg_2MnO_4, $MgMn_2O_4$ and $LiMn_2O_4$ [21,22]. Therefore, the present ion sieve shows a high adsorption capacity for Li^+ at higher pH. Additionally after adsorption, the measured final pH values decreases, which indicates that the HMS particles causes a release of H^+ into the solution under alkaline conditions. It dues to an occurrence of the Li^+–H^+ ion exchange reaction at the surface during the process of sorption of Li^+ onto HMS. This indicates that the higher solution pH helps to H^+ extraction and Li^+ insertion and increases Li^+ adsorption capacity consequently. What is more, it keeps coincident with the prediction from pH_{PZC} that at high pH the cation adsorption density increases.

3.5. Competitive adsorption model

According to the anterior results, the sorption of Li^+ is strongly pH-dependent and the level of lithium binding is influenced by H^+. So the competitive model is selected to fit the experimental data. This is based on the assumptions that sorption equilibrium can be expressed as

$$HMS + H^+ \rightleftharpoons HMS\text{–}H$$

$$HMS + Li^+ \rightleftharpoons HMS\text{–}Li$$

The results of experimental data for competitive adsorption model are depicted as a three-dimensional plot in Fig. 7. The parameters for model verification are also shown in Table 1. Low RMSE indicates high accuracy of the model in the prediction of sorption characteristics. The prediction for the maximum adsorption q_{max} is 4.89 mmol/g which is close to the experimental result. For the Li–H system, much higher values of the K parameter for Li than for H in the studied pH range 2–12 imply that the adsorbent has a higher affinity for Li than for H. Higher values of K are associated with a higher ratio of the desorption rate constant to the adsorption rate constant [38]. Accordingly, it is in line with the recycle of HMS which was studied before.

In Fig. 7, the final pHs increase from lower initial pHs. It dues that for the lower tested pH, it is reasonable that most of the sites are protonated and lithium ions cannot effectively compete with protons for the binding sites. An increase of the initial solution pH results in an increase of negatively charged sites and eventually an increase of metal ion binding. Li^+–H^+ ion exchange occurs simultaneously and it contributes to the decrease of pHs.

Table 1
Li–H binary system model fit results ($pH_{initial}$ = 2–12).

K_{Li} (mmol/L)	K_H (mmol/L)	q_{max} (mmol/g)	RMSE	SSE
1.41	0.0045	4.89	0.73	1.98

3.6. Adsorption kinetics

Effects of contact time and Li^+ concentration on adsorption of Li^+ by HMS are presented in Fig. 8. The amount of Li^+ adsorbed (mg/g) increases with increasing contact time. The extent of adsorption increases rapidly in the initial stages but becomes slow in the later stages till the attainment of equilibrium. Equilibrium time for the adsorption at various Li^+ concentrations is found to be 24 h, which

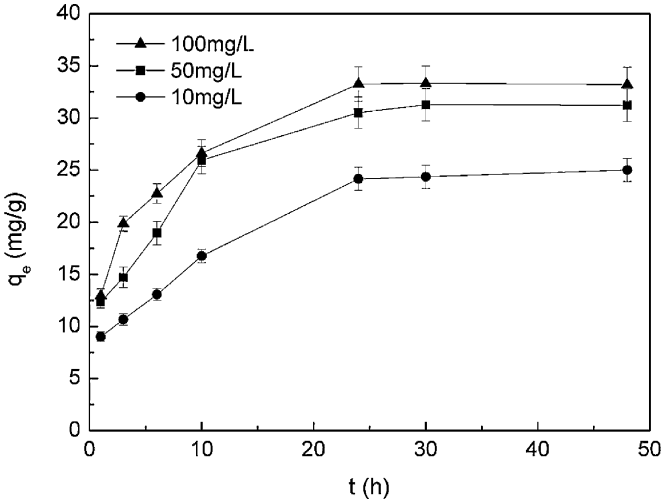

Fig. 8. Variation of Li^+ adsorption as a function of time and initial concentrations of the solution (T = 20 °C; m = 0.05 g; V = 250 mL; time, t = 1–48 h; C_0 = 10, 50, 100 mg/L; $pH_{initial}$ = 12).

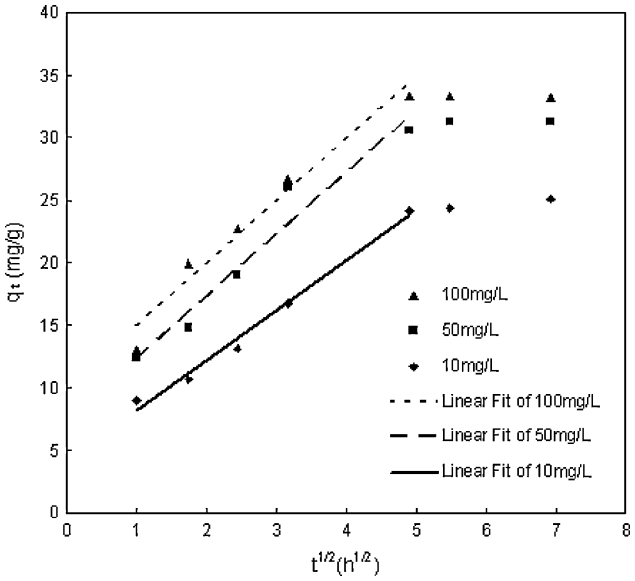

Fig. 9. Plots of intraparticle diffusion model of Li^+ onto HMS with different initial concentrations of Li^+.

shows that equilibrium time is independent of initial Li^+ concentration. The maximum of adsorption is found to be 25.01, 31.2 and 33.2 mg/g respectively. It also shows that the maximum of adsorption increases with the increase of initial concentration of Li^+.

For the purpose of understanding the sorption behavior of HMS, the intraparticle diffusion kinetic, pseudo-second-order and pseudo-first-order models are applied to the obtained data. The fitting data of pseudo-first-order are not shown here because of the lower correlation coefficients.

3.6.1. Intraparticle diffusion kinetics

According to the Weber–Morris model, the plot of q_t versus $t^{1/2}$ should be linear if intraparticle diffusion is involved in the adsorption system and if these lines pass through the origin, then intraparticle diffusion is the rate controlling step [39–42]. When the plots do not pass through the origin, this is indicative of some degree of boundary layer control, and this further indicates that intraparticle diffusion is not the only rate-limiting step, but also other kinetic models may control the rate of adsorption, all of which may be operating simultaneously. From Fig. 9, it can be seen that the plots of q_t versus $t^{1/2}$ do not pass through the origin. Therefore, intraparticle diffusion is not the only rate-limiting step. The correlation coefficients R^2 for the intraparticle diffusion model are explained in Table 2. This model indicates that adsorption of Li^+ onto HMS may be followed by an intraparticle diffusion model at the beginning of the adsorption.

3.6.2. Pseudo-second-order kinetics

Plots of the pseudo-second-order model at different initial Li^+ concentrations are presented in Fig. 10. The constants calculated from the slope and intercept of the plots are given in Table 3. It can be seen that R^2 values are greater than 0.99. Additionally, low RMSE values and SSE indicate that theoretical and experimental q_e values are in a good accordance with each other. Therefore, it is possible to suggest that the sorption of Li^+ onto HMS is the second-order

Table 2
The rate parameters of HMS for intraparticle diffusion kinetic model.

$C_{(Li^+)}$ (mg/L)	10	50	100
k_{WM} (mg/h)	4.00	4.97	4.98
R^2	0.9873	0.9499	0.9654

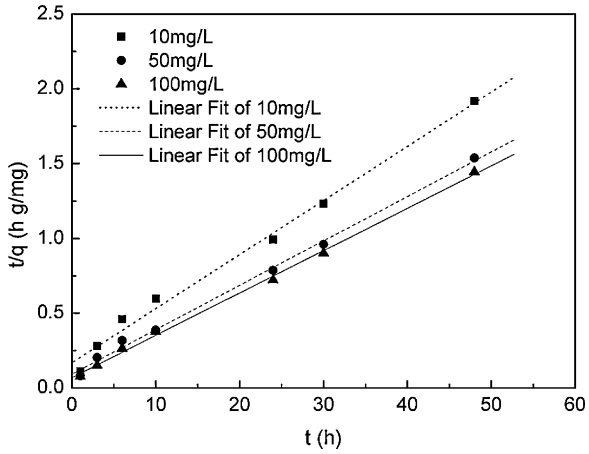

Fig. 10. Plots of the pseudo-second-order kinetic model at different initial Li^+ concentration.

Table 3
The rate parameters of HMS for pseudo-second-order kinetic model.

C (mg/L)	q_{exp} (mg/g)	q_e (mg/g)	k_2 (g/mg h)	R^2	RMSE	SSE
10	25.01	27.62	0.0078	0.9965	0.065	0.0210
50	31.21	34.36	0.0092	0.9911	0.034	0.0056
100	33.20	35.33	0.0120	0.9980	0.024	0.0029

reaction based on the assumption that the rate-limiting step may be chemical sorption [43]. The result is similar to the ion sieve from lithium manganese oxide reported by Wang et al. [32].

4. Conclusions

The characteristics and adsorption properties of Mg^{2+} doped spinel lithium ion sieve were studied. The followed conclusions can be summarized.

(1) The lithium ion sieve (HMS) obtained from Mg^{2+} doped spinel lithium manganese oxide preserved the original spinel structure. Scanning electron microscopy (SEM) image and transmission electron microscopy (TEM) image showed that the HMS grains presented as the cluster form of floccules and nanosized particles. The determination of pH_{PZC} was 7.8 and showed an amphoteric surface. There exist electrostatic forces during the sorption of Li^+ onto HMS in addition to the main ion-exchange mechanism.
(2) The batch experiment results suggested that the sorption of Li^+ showed a highly pH and initial concentration dependent profile. The adsorption capacity increased with the increase of initial pH and concentration and reached up to 37.4 mg/g at pH 12 with initial concentration 200 mg/L. The adsorption capacity remained above 95% after reused for 4 times.
(3) Three-dimensional sorption surfaces using parameters derived from this model could be used to predict the effects of pH on Li^+ adsorption over a continuum of pH values.
(4) Kinetic experiments suggested that the adsorption process followed the pseudo-second-order model and at the beginning, the adsorption of Li^+ onto HMS may be followed by an intraparticle diffusion model.

References

[1] J.S. Yuan, Z.Y. Ji, The progress of extracting lithium from seawater, Chin. Sea-Lake Salt Chem. Ind. 32 (2003) 29–33.
[2] R. Chitrakar, H. Kanoh, Y. Miyai, K. Ooi, Recovery of lithium from seawater using manganese oxide adsorbent ($H_{1.6}Mn_{1.6}O_4$) derived from $Li_{1.6}Mn_{1.6}O_4$, Ind. Eng. Chem. Res. 40 (2001) 2054–2058.

[3] Y.Q. Fan, X.X. Jiang, S.D. Wang, L. Zhao, L.Y. Feng, Study on modification of deep-sea manganese nodules to adsorb lithium ion, Mining Metall. 3 (2008) 41–45.
[4] M. Abe, R. Chitrakar, Recovery of lithium from seawater and hydrothermal water by titanium (IV) antimonate cation exchanger, Hydrometallurgy 19 (1987) 117–128.
[5] B. Ammundsen, P.B. Aitchison, G.R. Burns, D.J. Jones, J. Roziere, Proton insertion and lithium-proton exchange in spinel lithium manganates, Solid State Ionics 97 (1997) 269–276.
[6] R. Chitrakar, H. Kanoh, Y. Miyai, K. Ooi, A new type of manganese oxide $MnO_2{\cdot}0.5H_2O$ derived from $Li_{1.6}Mn_{1.6}O_4$ and its lithium ion-sieve properties, Chem. Mater. 12 (2000) 3151–3157.
[7] X.J. Yang, H. Kanoh, W.P. Tang, K. Ooi, Synthesis of $Li_{1.33}Mn_{1.67}O_4$ spinels with different morphologies and their ion adsorptivities after delithiation, J. Mater. Chem. 10 (2000) 1903–1909.
[8] J.C. Hunter, Preparation of a new crystal form of manganese dioxide: λ-MnO_2, J. Solid State Chem. 39 (1981) 142–147.
[9] K. Ooi, Y. Miyai, S. Katoh, H. Maeda, M. Abe, Topotactic Li^+ insertion to λ-MnO_2 in the aqueous phase, Langmuir 5 (1989) 150–157.
[10] X.M. Shen, A. Clearfield, Phase transitions and ion exchange behavior of electrolytically prepared manganese dioxide, J. Solid State Chem. 64 (1986) 270–282.
[11] Q. Feng, Y. Miyai, H. Kanoh, K. Ooi, Li^+ extraction/insertion with spinel-type lithium manganese oxides. Characterization of redox-type and ion-exchange-type sites, Langmuir 8 (1992) 1861–1867.
[12] G.M. Song, Z.M. Xu, Y.J. Wang, Y. Zhou, Synthesis and electrochemical characterization of $LiMn_{2-x}Al_xO_4$ powders prepared by mechanical alloying and rotary heating, Electrochem. Commun. 5 (2003) 907–912.
[13] Y.K. Sun, Structural degradation mechanism of oxysulfide spinel $LiAl_{0.24}Mn_{1.76}O_{3.98}S_{0.02}$ cathode materials on high temperature cycling, Electrochim. Commun. 3 (2001) 199–202.
[14] D. Song, H. Ikuta, T. Uchida, M. Wakihara, The spinel phases $LiAl_yMn_{2-y}O_4$ (y = 0, 1/12, 1/9, 1/6, 1/3) and $Li(Al,M)_{1/6}Mn_{11/6}O_4$ (M = Cr, Co) as the cathode for rechargeable lithium batteries, Solid State Ionics 117 (1999) 151–156.
[15] Y.S. Lee, N. Kumada, M. Yoshio, Synthesis and characterization of lithium aluminum-doped spinel ($LiAl_xMn_{2-x}O_4$) for lithium secondary battery, J. Power Sources 96 (2001) 376–384.
[16] Y.S. Lee, M. Yoshio, Effect of Mn source and peculiar cycle characterization, Solid-State Lett. 4 (2001) A155–A158.
[17] S.T. Myung, S. Komaba, N. Kumagai, Enhanced structural stability and cyclability of Al-doped, J. Electrochem. Soc. 148 (2001) A482–A489.
[18] Q. Feng, Y. Miyai, H. Kanoh, K. Ooi, Li^+ and Mg^{2+} extraction and Li^+ insertion reactions with $LiMg_{0.5}Mn_{1.5}O_4$ spinel in the aqueous phase, Chem. Mater. 5 (1993) 311–316.
[19] Y.F. Liu, Q. Feng, K. Ooi, Li^+ extraction/insertion reactions with $LiAlMnO_4$ and $LiFeMnO_4$ spinels in the aqueous phase, J. Colloid Interface Sci. 163 (1994) 130–136.
[20] R. Chitrakar, H. Kanoh, Y. Makita, Y. Miyai, K. Ooi, Synthesis of spinel-type lithium antimony manganese oxides and their Li^+ extraction/ion insertion reactions, J. Mater. Chem. 10 (2000) 2325–2329.
[21] Y. Miyai, K. Ooi, S. Katoh, Recovery of lithium from seawater using a new type of ion-sieve adsorbent based on $MgMn_2O_4$, Sep. Sci. Technol. 23 (1988) 187–199.
[22] Y. Miyai, K. Ooi, S. Katoh, Preparation and ion-exchange properties of ion-sieve manganese oxide based on Mg_2MnO_4, J. Colloid Interface Sci. 130 (1989) 535–541.
[23] L. Wang, W. Ma, R. Liu, H.Y. Li, C.G. Meng, Correlation between Li^+ adsorption capacity and the preparation conditions of spinel lithium manganese precursor, Solid State Ionics 177 (2006) 1421–1428.
[24] G. Newcombe, R. Hayes, M. Drikas, Granular activated carbon: importance of surface properties in the adsorption of naturally occurring organics, Colloids Surf. A 78 (1993) 65–71.
[25] S. Yiacoumi, J. Chen, Modeling of metal ion sorption phenomena in environmental systems, Stud. Surf. Sci. Catal. 120B (1999) 285–317.
[26] S. Schiewer, M.H. Wong, Metal binding stoichiometry and isotherm choice in biosorption, Environ. Sci. Technol. 33 (1999) 3821–3828.
[27] W. Ma, J.M. Tobin, Determination and modeling of effects of pH on peat biosorption of chromium, copper and cadmium, Biochem. Eng. J. 18 (2004) 33–40.
[28] T. Akar, B. Anilan, Z. Kaynak, A. Gorgulu, S.T. Akar, Batch and dynamic flow biosorption potential of agaricus bisporus/thuja orientalis biomass mixture for decolorization of RR45 dye, Ind. Eng. Chem. Res. 47 (2008) 9715–9723.
[29] C. Namasivayam, S. Sumithra, Adsorptive removal of catechol on waste Fe(III)/Cr(III) hydroxide: equilibrium and kinetics study, Ind. Eng. Chem. Res. 43 (2004) 7581–7587.
[30] K. Vijayaraghavan, T.V.N. Padmesh, K. Palanivelu, M. Velan, Biosorption of nickel (II) ions onto sargassum wightii: application of two-parameter and three-parameter isotherm models, J. Hazard. Mater. 133 (2006) 304–308.
[31] G. Ahmet, Application of nonlinear regression analysis for ammonium exchange by natural (Bigadic) clinoptilolite, J. Hazard. Mater. 148 (2007) 708–713.
[32] L. Wang, C.G. Meng, M. Han, W. Ma, Lithium uptake in fixed-pH solution by ion sieves, J. Colloid Interface Sci. 325 (2008) 31–40.
[33] A. Fernandez-Nieves, C. Richter, F.J. De las Nieves, Point of zero charge (PZC) estimation for a TiO_2/water interface, Prog. Colloid Polym. Sci., Trends Colloid Interface Sci. XII, 21, 1998.
[34] I.D. Smiciklas, S.K. Milonjic, P. Pfendt, S. Raicevic, The point of zero charge and sorption of cadmium (II) and strontium (II) ions on synthetic hydroxyapatite, Sep. Purif. Technol. 18 (2000) 185–194.
[35] Z. Chen, W. Ma, M. Han, Biosorption of nickel and copper onto treated alga (*Undaria pinnatifida*): application of isotherm and kinetic models, J. Hazard. Mater. 155 (2008) 327–333.
[36] T.C. Tan, W.K. Teo, Combined effect of carbon dosage and initial adsorbate concentration on the adsorption isotherm of heavy metals on activated carbon, Water Res. 21 (1987) 1183–1188.
[37] A. Ahmad, M. Rafatullah, O. Sulaiman, M.H. Ibrahim, Y.Y. Chii, B.M. Siddique, Removal of Cu(II) and Pb(II) ions from aqueous solutions by adsorption on sawdust of Meranti wood, Desalination 247 (2009) 636–646.
[38] K.H. Chong, B. Volesky, Description of two-metal biosorption equilibria by Langmuir-type models, Biotechnol. Bioeng. 47 (1995) 451–460.
[39] N. Kannan, M.M. Sundaram, Kinetics and mechanism of removal of methylene blue by adsorption on various carbons—a comparative study, Dyes Pigments 51 (2001) 25–40.
[40] T.D. Khokhlova, Y.S. Nikitin, A.L. Detistova, Modification of silicas and their investigation by dye adsorption, Adsorp. Sci. Technol. 15 (1997) 333–340.
[41] W.T. Tsai, K.J. Hsien, J.M. Yang, Silica adsorbent prepared from spent diatomaceous earth and its application to removal of dye from aqueous solution, J. Colloid Interface Sci. 275 (2004) 428–433.
[42] K.R. Ramakrishna, T. Viraraghavan, Use of slag for dye removal, Waste Manage. 17 (1998) 483–488.
[43] Y.S. Ho, G. McKay, Pseudo-second order model for sorption processes, Process Biochem. 34 (1999) 451–465.